**Evaluation of Implicit Solvent Models in Molecular Dynamics Simulation of α-Synuclein**

Loizos Savva and James A. Platts*
School of Chemistry, Cardiff University, Park Place, Cardiff CF10 3AT, UK.

* Author for correspondence: platts@cardiff.ac.uk +44-2920-874950

**Abstract**

We report conventional and accelerated molecular dynamics simulations of α-Synuclein, designed to assess performance of using different starting conformation, solvation environment and force field combination. Backbone and sidechain chemical shifts, radius of gyration, presence of β-hairpin structures in KTK(E/Q)GV repeats and secondary structure percentages were used to evaluate how variations in forcefield, solvation model and simulation protocol provide results that correlate with experimental findings. We show that with suitable choice of forcefield and solvent, ff03ws and OBC implicit model, respectively, acceptable reproduction of experimental data on size and secondary structure is obtained by both conventional and accelerated MD. In contrast to the implicit solvent model, simulations in explicit TIP4P/2005 solvent do not properly represent size or secondary structure of α-Synuclein.

**Keywords** Parkinson's disease; synuclein; molecular dynamics; implicit solvent; β-hairpins

## Introduction

Parkinson's disease (PD) is one of the most common neurodegenerative disorders. It is classed as a synucleinopathy, where pathogenesis is attributed to α-Synuclein (αS) aggregation into amyloid fibrils, resulting in neuronal dysfunction. This peptide is also believed to be involved to an extent with Alzheimer's disease (AD) pathogenesis, and has been found to accumulate in senile plaques, specifically in the hydrophobic non-Aβ component (NAC) found in the central region of the peptide, between residues 61 and 95, as illustrated in Figure 1.[1] αS belongs in the family of intrinsically disordered proteins (IDPs), displaying unpredictable conformational assemblies.

Studies on IDPs and the processes these are involved in, have gained traction over the last 20 years, with reports on how their inherent spatio-temporal heterogeneity may be regulated, varied and influenced by their environment.[2] Despite their name, IDPs generally display a degree of function-related structural configuration, with retention times ranging depending on the peptide.[3] α-Synuclein fibril formation involves various intermediates, with the peptide undergoing many structural transitions, of which some could offer possible structural assemblies that facilitate aggregation. Experimental evidence on the folding inclinations of the peptide indicate that KTK(E/Q)GV residue repeats which start in the N-terminus and extend to the NAC region of the peptide may be responsible for the formation of cross β-sheets, promoting the development of fibrils.[4,5]

Biophysical studies, employing nuclear magnetic resonance (NMR),[6,7] small angle X-ray scattering (SAXS),[8–10] circular dichroism (CD),[11–14] and Raman[15,16] and Attenuated Total Reflection Fourier Transform Infrared (ATR-FTIR) spectroscopic techniques,[17] have attempted to characterise the peptide's structure. The principal goal of these studies has been to reveal how the structural assembly of monomeric systems relates to the formation of fibrils, which have been associated with PD.[18] Thus, evaluating the percentage of different secondary characteristics, as well as the overall compactness of the peptide through radius of gyration, ultimately aiming to relate the propensity of α-synuclein to form aggregates, with folding features expressed through the different techniques. The experimental evidence available in the literature present a range of secondary structure percentage, depending on the technique used, something to be expected considering the disordered nature of αS. Nevertheless, some of the characteristics that remain relatively constant, despite the variance seen in secondary structure, has been the radius of gyration, ranging between 35-40 Å, as well as the presence of β-hairpins, formed within the residue repeats involved in the intermediates during the fibrillation process.[7,11,12,14,19,20]

One can see how molecular dynamic (MD) simulations offer the ability to obtain a great insight into the structural development and evolution of this disordered peptide within a timeframe, permitting the analysis of a time-associated ensemble of conformations, rather than looking at an averaged examination of the characteristics, which is the case in experimental studies. Notwithstanding the availability of computational studies on this peptide, the majority of them have been focusing on simulations in explicit solvent, resulting in more compact structures with lower $R_g$ values than those found experimentally.[21–24] The significant computational cost of simulations in explicit solvent needs to be considered, especially when looking at systems that involve a large, flexible peptide requiring a large water box, such as the case here, particularly if starting from an extended conformation. The confined solvent volume has been reported to affect the simulations of IDPs,[25] indicating the susceptibility of the systems to the effects of explicit solvent environment.

Implicit solvent studies have been reported on replica exchange molecular dynamic (REMD), as well as conventional MD (cMD) simulations,[21,26,27] where the ff99SB force field had been used, alongside the Onufriev-Bashford-Case (OBC) and generalized Born (GB) implicit solvents, for relatively short trajectories in the nanosecond scale. In those studies, the case for implicit solvent simulations on αS had been made, also through a direct comparison with explicit simulations,[21,26] concluding that the advantages of using a continuum solvent model shouldn't be disregarded because of the lack of intermolecular interactions with the surrounding environment, as implicit simulations benefit from not being confined by the solvent box size. The selection of force field requires consideration of the intrinsically disordered nature of the peptide: we therefore concentrate on force fields employed in explicit and implicit solvent simulations of synuclein and other IDPs.[21,28,29]

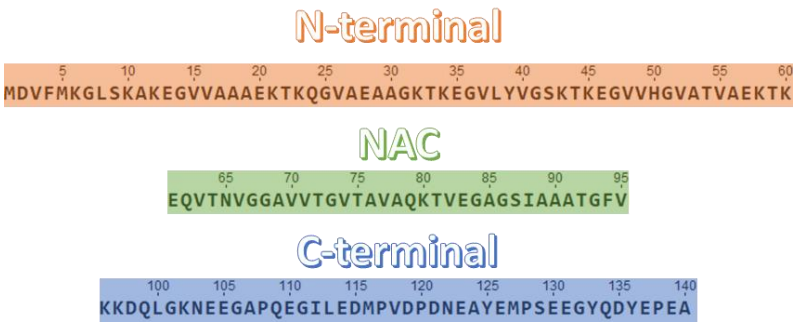


Figure 1 Primary structure, showing the three main regions of αS.

**Computational Methods**

The molecular dynamic simulations for this study were carried out using the AMBER16 package.[30] The peptide was simulated with the ff03ws and ff14SB force fields. The choice of force field was made after considering our previous evaluation of ff14SB with the generalised Born surface area (GBSA), for use with biomolecular systems.[31] The peptide simulated with ff03ws was solvated with the TIP4P/2005 explicit solvent model,[32] as well as the Onufriev, Bashford, Case (OBC) modification to the generalised Born (GB) model.[33–35] The choice of the ff03ws force field was made after looking at its performance with IDPs, accurately reproducing experimental observations from small-angle X-ray scattering (SAXS),[36,37] and nuclear magnetic resonance (NMR) studies.[38] Although the studies that implemented the ff03ws for simulations of αS, were done using explicit solvent, the performance of the ff03 force field,[39] coupled with the OBC implicit solvent, has been well documented in the literature.[40–45] Acknowledging the backbone corrections, made to refine the force field for use with the TIP4P/2005 explicit solvent in ff03w, and additional scaling in ff03ws, the force field was kept the same, both in the explicit and implicit simulations. Although the specific combination of ff03ws and OBC has not been reported before, we show below that it results in acceptable reproduction of experimental data.

An initial assessment was performed on the starting conformation, where the peptide was simulated with two starting conformations – an experimentally defined structure from an NMR study on αS confined in a micelle,[46] and a fully extended conformation modelled manually in MOE.[47] After minimisation, conventional molecular dynamics (cMD) simulations were performed for 150 million steps, at a 2 fs timestep, resulting in 300 ns worth of data. The NVT ensemble was employed at 310 K, with the Langevin thermostat.[48] SHAKE[49] holonomic constraints were imposed on bonds to hydrogen, restraining them to their equilibrium length. After examining the root mean square deviation (RMSD) and radius of gyration ($R_g$) plots from the whole trajectory, 50 ns were discounted from the beginning of the trajectory to account for equilibration of trajectories.

The MD simulations performed here may be split into three simulation scenarios: 1) for the evaluation of the starting conformation and force field, conventional MD were performed for 300 ns, with the initial 50 ns discarded as equilibration steps; 2) explicit solvent simulation was performed on a single 300 ns cMD trajectory; 3) having performed the initial assessment, conventional and accelerated MD (aMD) simulations, in implicit solvent, were completed in sets of 3 individual runs of 600 ns each, again with the initial 50 ns of cMD discarded for equilibration.

The explicit solvent used with the chosen force field, was TIP4P/2005,[32] after considering its performance in biological systems,[50] as well as the force field's optimisation around that specific water model,[28] as well as the sole use of that explicit solvent with ff03ws, in other computational studies.[37,51–54] TIP4P and TIP4P-D explicit solvent models were also tested, under the reported parameterisation, although the results obtained with either of those proved less capable in providing structural characteristics close to experimental values, thus are not reported here. The final structure from 300 ns implicit solvent simulation was used as the starting point for explicit solvent simulation, considering the significantly larger water box required to simulate the dynamics starting from an extended conformation. A periodic solvent box was built, using LEaP, with minimum of 50 Å between the atoms of the peptide and the box edge. The large distance of the water box was chosen, having tested 20 and 35 Å, to avoid interaction with neighbouring simulation boxes, while also allowing extended conformations to form during the simulation.[55] This run was limited to a single 300 ns trajectory, due to the increased computational demand of such simulation. Equilibration of explicit solvent simulations first employed the NPT ensemble for 8 ns at a cutoff of 10 Å and 2 fs timestep, with the Monte Carlo barostat at a pressure of 1 bar. This was followed by NVT simulation for 100 ns at a cutoff of 10 Å and 2 fs timestep, with Langevin dynamics for temperature scaling at 310 K and a collision frequency of $\gamma = 2.0$, before moving to the production run, in the NVT ensemble.

Having obtained the data from the conventional MD simulations in implicit solvent, an enhanced sampling of the phase space was performed using accelerated MD.[56] The mean total potential and dihedral energies, from the three 600 ns implicit solvent trajectories, were used to impose a bias on the system, using a boost potential, pushing the system to unexplored local minima positions. The aMD simulations were a continuation on the initial three cMD trajectories, each with their own final velocity and conformation. The enhanced sampling achieved using aMD, permits the sampling of trajectories that would remain uncharted by standard MD. The free energy landscape and original ensembles are hence recovered, through reweighting.[56] The cpptraj[57] analysis tool was used to obtain data on the secondary structure, RMSD, $R_g$, root mean square fluctuation (RMSF), salt bridges, hydrogen bonds and free energy landscapes, from these simulations.

## Results and Discussion

### *Evaluation of force field and starting conformation*

The peptide was initially simulated in implicit solvent, with two starting conformations – one already folded in a horseshoe-like configuration, from an NMR experiment where the peptide was studied in a micelle,[46] and the other in an extended form. Having performed 300 ns conventional MD simulations on the four systems, the first 50 ns were discounted, being regarded as equilibration steps. The decision on the length of the trajectory that needed to be removed as equilibration was made after inspection of $R_g$ and RMSD data, as shown in Figure 2. Henceforth the data analysed shall only include values after the equilibration steps have been removed.

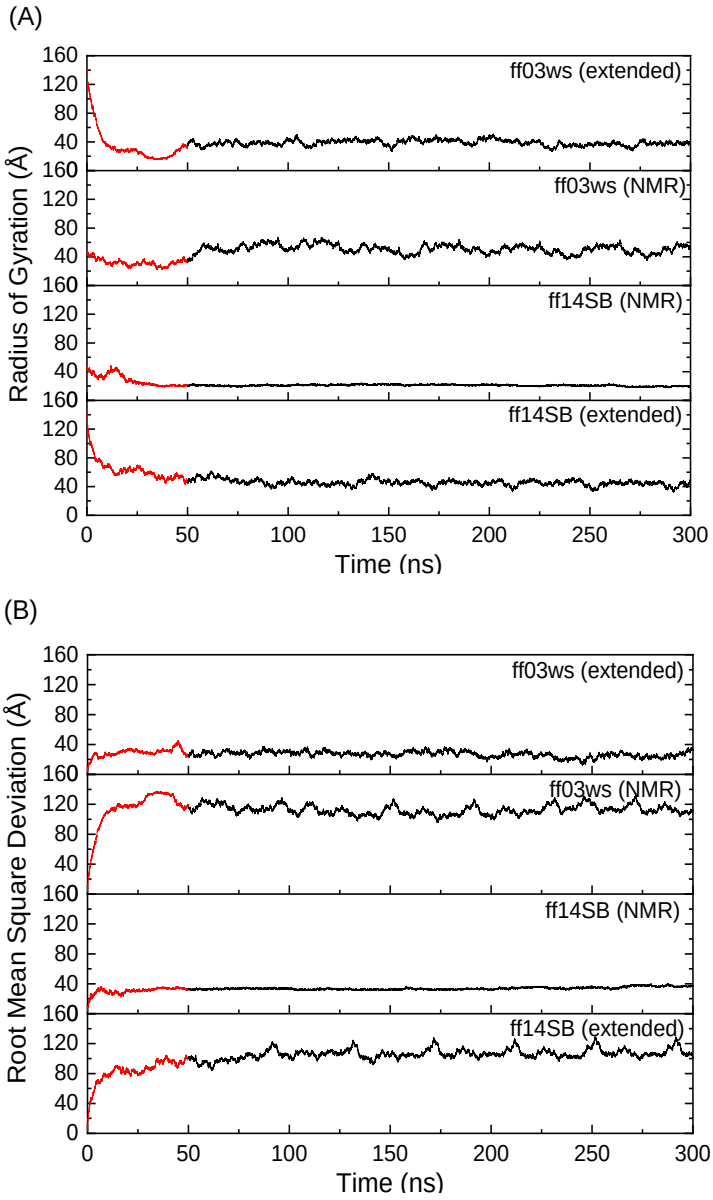


Figure 2 (A) Radius of gyration and (B) root mean square deviation (RMSD) plots, showing the change from equilibration (red) to conventional MD (black), for the different systems studied.

The secondary structural characterisation of α-Synuclein has been elusive in experimental studies, owing to its highly disordered nature. The general consensus amongst research involving this peptide, has been that the lack of a defined structure, makes it hard to identify a structure-function relationship.[16,58] The majority of studies surrounding the characterisation of the peptide, primarily rely on results from circular dichroism (CD) spectroscopy. A survey of the reported characteristics from literature studies is given below in Table 1.

Table 1 Literature survey of reported secondary structural characteristics from different experimental methods.

| Method | Reference | Conditions | α-helix (%) | β-strand (%) | Other (%) |
|---|---|---|---|---|---|
| Circular Dichroism | [11] | Untreated αS (0.074 mg/mL), 293.15 K, pH 7.4 | 2±3 | 11±7 | 86±22 |
| | [12] | αS (0.2 mg/mL), Tris-HCl (25 mM), NaCl (50 mM), 293.15 K, pH 7.4 | ~0 | 31 | 68 |
| | [13] | purified αS from mouse brain (7.5 μM), PBS[a] (25%), 293.15 K, pH 7.4 | 22.5±1.5 | n/a | 46.5±12.5 |
| | [14] | αS (2.0 mg/mL), PBS[a] (100 mM), NaCl (100 mM), pH 7.4 | 19±1 | n/a | n/a |
| Raman Spectroscopy | [15] | αS (200 μM), Tris-HCl (20 mM), pH 7.5 | 49 | 10 | 41 |
| | [16] | αS (300 μM), PBS[a] (20 mM), pH 7.5 | 48 | 15 | 37 |
| ATR-FTIR Spectroscopy | [17] | Supernatant αS {from lyophilized sample (2-5 mg) dissolved in dd$H_2O$, NaOH (100 mM), pH 10±0.5, incubated at 293.15 K and centrifuged for 30 min}, HCl (1 mM), Tris-HCl, pH 7.4 | 35 | 3 | 62 |

[a] Phosphate-buffered saline

The variability in the characteristics of the peptide, along with the general uncertainty that surrounds the reported secondary structure of αS in the literature, makes it hard to use such values to assess the validity of simulation methodologies. Despite the discrepancies encountered from the use of different methods, the changes in the secondary structure, from alterations in the conditions and the environment in which the peptide is modelled in, can still be evaluated.

Perhaps a better approach for assessing the structural characteristics of αS is through backbone and sidechain C NMR chemical shifts, which provide more easily reproducible predictions on the local covalent interactions within the peptide. The values for the chemical shifts were obtained through SPARTA+.[59] The predicted chemical shifts derived from deviations of Cα and Cβ from their random coil values, are given in Figure 3, with the predicted Cα chemical shift values obtained from the simulations, plotted against experimental data, given in Figure 4 (full data in Supporting Information).[60] The plots point towards the ff03ws/OBC combination, to give the structure that more closely resembles experimental NMR predictions, particularly where the two termini are concerned, closely matching residues 10-21 and 114-131, in the negative region which they appear, Figure 3, indicating a propensity for β-sheets.[61] These observations correlate with the predicted Cα chemical shift values, showing a close resemblance to the experimental predictions throughout, but in particular in the two termini, with mean percentage error for the N- and C-termini at 1.73% and 1.98%, respectively, and 2.35% for the NAC region, totalling a 1.97% mean error for the whole peptide. These values increase all through the peptide simulated with the ff14SB/GBSA parameterisation, raising the mean error to 2.62%, with the three individual regions averaging values between 2.52% and 2.74%, Table S2.

Further key characteristics, that correlate to experimental findings, include the presence of a combination of positive and negative shifts, representing α- and β-characteristics, respectively, in the N-terminal region of the peptide, with the C-terminal consisting mainly of β-character, and the NAC region of the peptide presenting a combination of the two structures.[61,62] The lack of serial negative chemical shifts in the core regions, as well as the N-terminus, of the ff14SB plot, brings into question the assessment of β-structures using this force field.

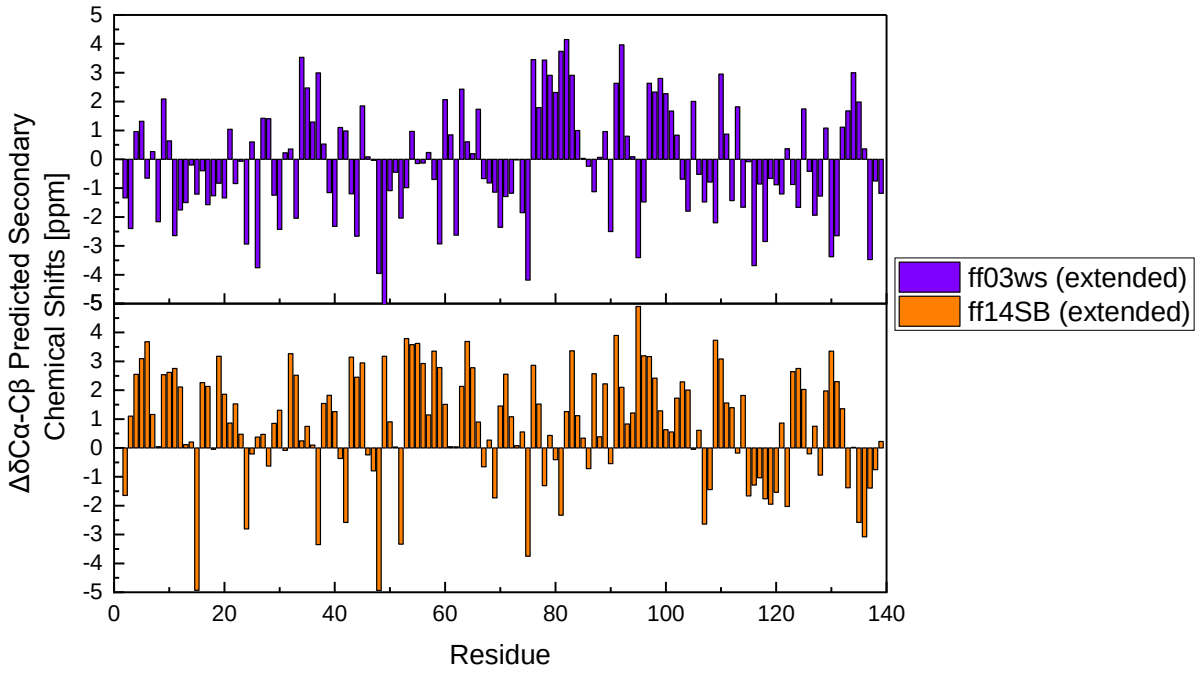


Figure 3 Deviation of Cα-Cβ chemical shifts from their random coil values. The results consist of 1250 frames, taken from conventional MD simulations of αS, starting from extended conformation.

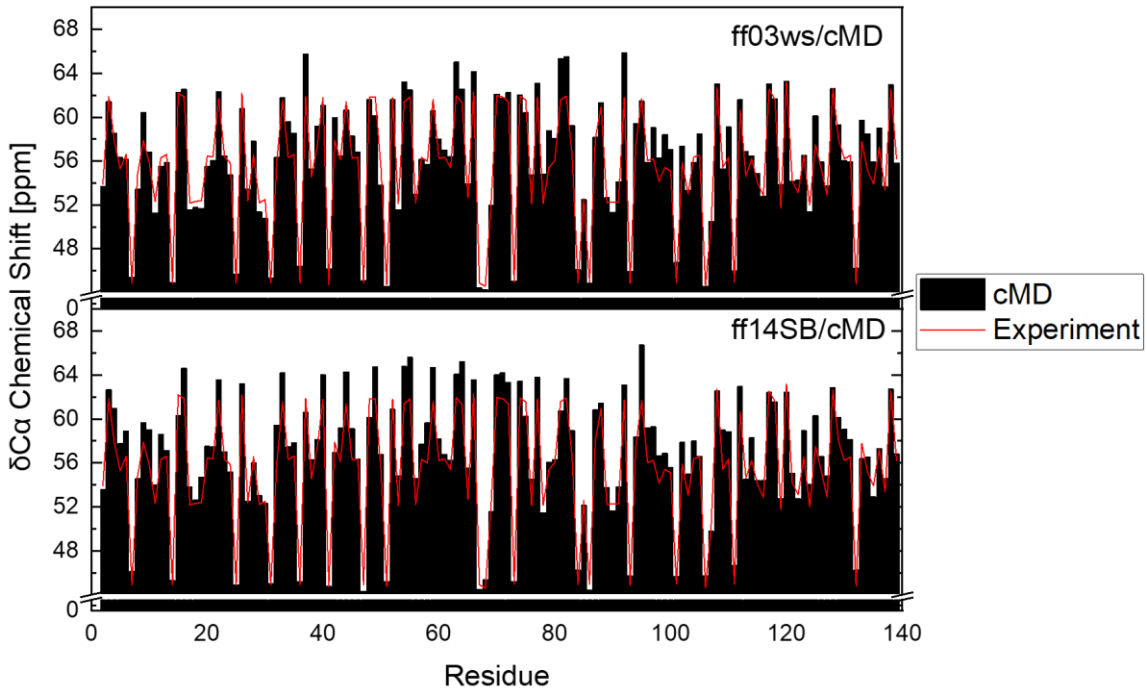


Figure 4 Predicted Cα chemical shift values per residue, from 1250 frames taken from the conventional MD simulations on αS (black), using different force field/solvent combinations, starting from the extended conformation. Experimental data (red) obtained from source.[60]

Specific motifs that appear in residue repeats have also been used here, alongside radius of gyration, to corroborate experimental and computational observations. The greatest contribution of secondary structural characteristics, and in particular β-sheets through the formation of β-hairpins, has been found in or around the KTK(E/Q)GV repeats (between residues 21-26, 32-37 and 43-48); starting from the N-terminal region and extending into the NAC, through KTKEQV at positions 58-63, which has been reported to have a great influence on the stability of the NAC region.[19] These regions have also been reported in the past to be involved in the compact topological arrangement in α-Synuclein, while also being present in other forms of synuclein.[7,20] The contribution of these repeats, along with the residues surrounding them, in the overall folding of the peptide can also be seen from the salt bridges formed between the Lys and Glu residues contained within these regions (*vide infra*, Figure 8). These β-hairpin structures occur through the formation of anti-parallel β-sheets, Figure 5 and Figure 6. Similar β-hairpin structures have also been observed here between residues 63-72, existing in a more permanent fashion. These locations have been primarily taken into consideration when evaluating the efficacy of the force fields to simulate trajectories that come in agreement with experimental findings as constitute the most well defined characteristic of synucleins.

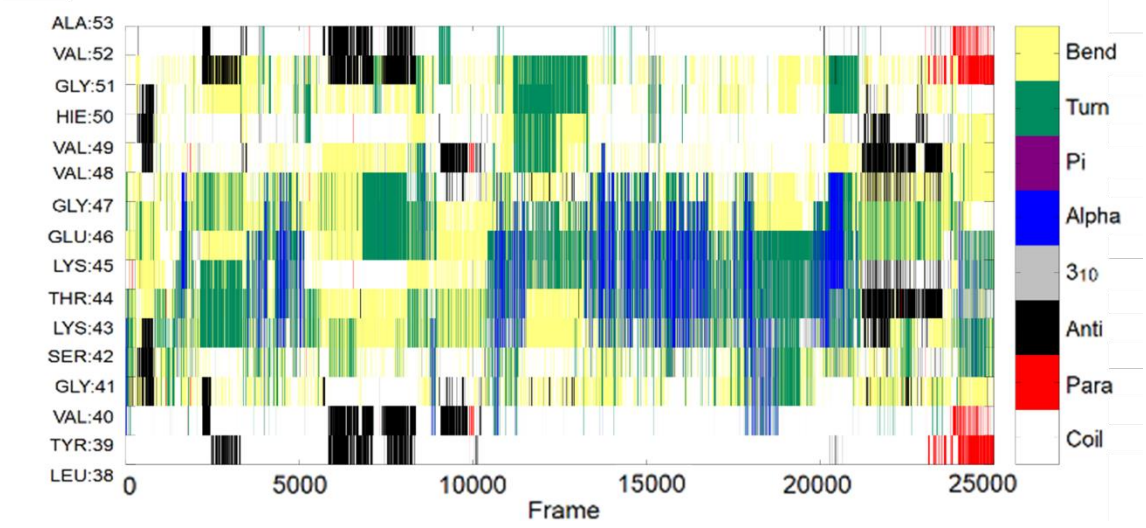


Figure 5 Evolution of secondary structure characteristics of each of the residues in the hairpin region, found within the peptide over the length of the conventional MD trajectory, using **ff03ws/OBC** from the extended starting conformation. The antiparallel (black) β-sheets with turn/bend (yellow/green) between indicate possible presence of β-hairpin.

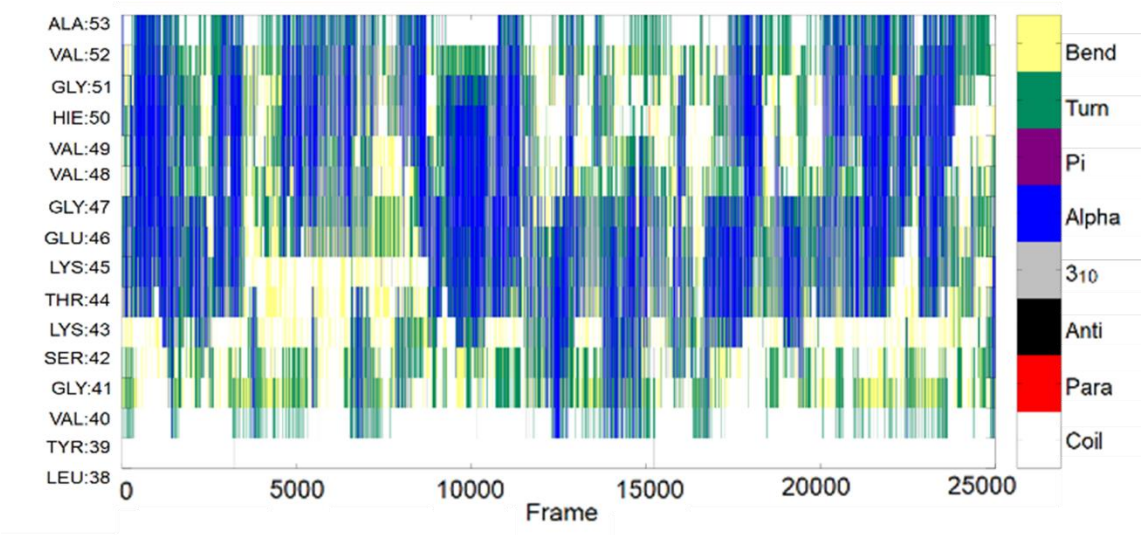


Figure 6 Evolution of secondary structure characteristics of each of the residues in the hairpin region, found within the peptide over the length of the conventional MD trajectory, using **ff14SB/GBSA** from the extended starting conformation. The lack of antiparallel β-sheets suggests the absence of β-hairpins in this system.

Secondary structure as a function of residue are shown in Figure 7, with a numerical representation of the overall percentages in Table 2, and a breakdown of the secondary structure contribution of the two termini and central NAC regions in Table 3. From the data presented here, it is evident that the central region of the peptide accounts for the highest percentage of β-character in the overall system. The most discernible observation that may be made on the difference of the three systems, is the lack of β-characteristics with ff14SB, especially where the extended starting conformation is concerned where it only accounts for 0.12% of the secondary characteristics, preferring the helical and coiled structural arrangement. The overestimation of α-helical character when using ff14SB, at least where IDPs are concerned, has already been reported in the literature,[63] with the evidence presented here further supporting the questionable suitability of this force field to accurately predict the secondary structure characteristics of disordered systems.

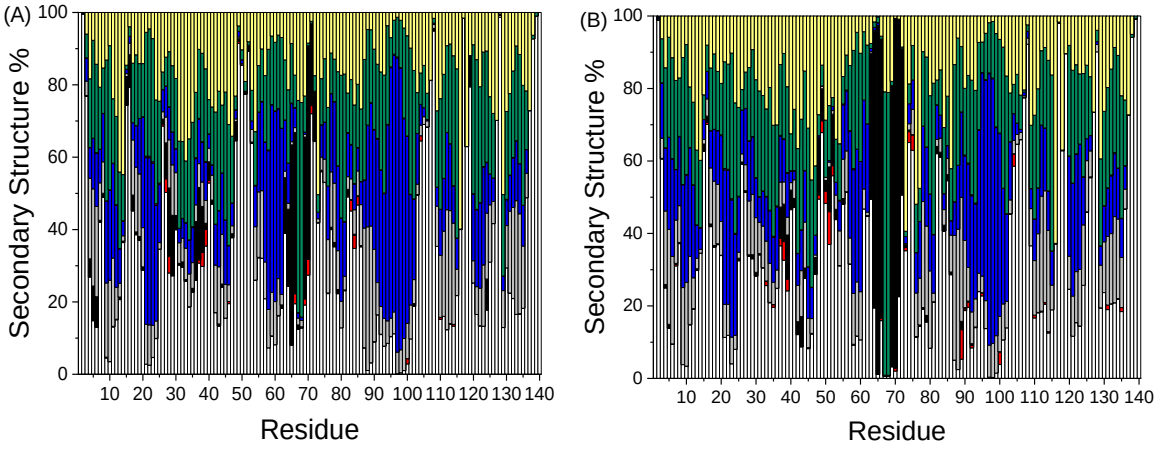

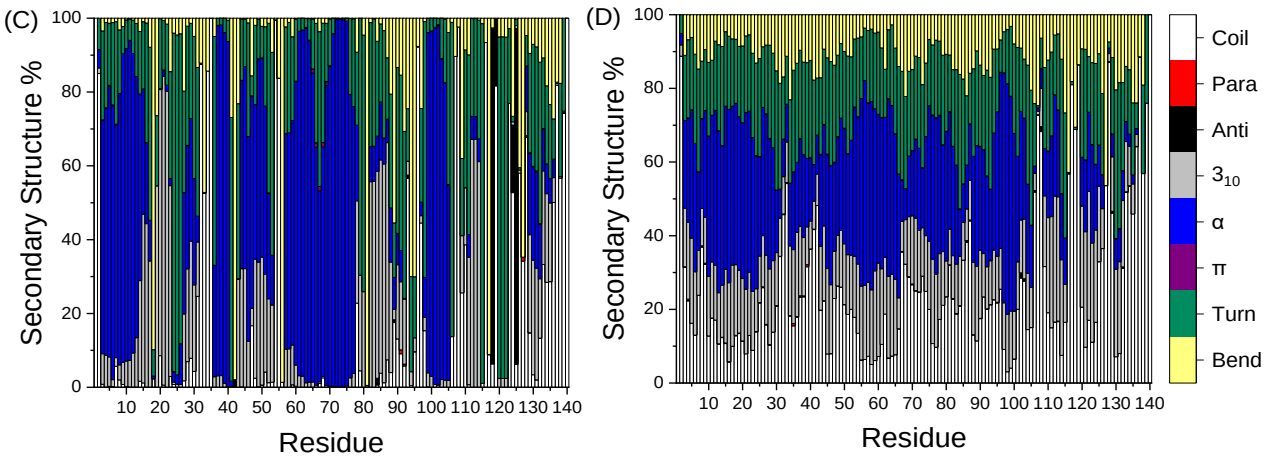


Figure 7 Secondary structure distribution per residue after 250 ns cMD using ff03ws with (A) NMR-defined and (B) extended starting conformations, and ff14SB with (C) NMR-defined and (D) extended starting conformations. The β-sheets are denoted with red (parallel) and black (antiparallel), while the α-helices with grey ($3_{10}$), blue (α) and purple (π).

Evaluating the similarities of the secondary structures obtained from the different force fields and starting conformations, to the experimental values presented in Table 1, a clear distinction can be made on the superiority of the values obtained with ff03ws over ff14SB. This is largely due to the lack of β-character in the latter, which evidently is not the case in any experimental data. In particular, looking at the ATR-FTIR spectroscopic results,[17] acceptable reproduction of the experimental values was achieved with the ff03ws simulations, with β-sheet percentages ranging between 3.5-6% and α-helices between 24-26%, compared to 3% and 35% β- and α-characteristics, respectively, reported from the experiment. The overestimation of α-helices in the ff14SB simulations is in accord with the Raman spectroscopic results,[15,16] although the near-null values of β-sheet character, compared to the reported 10-15% experimental value, brings the validity of the force field into question.

A closer evaluation of the secondary structures found in the three main regions of the peptide, is presented in Table 3. The systems simulated with ff03ws/OBC appear to follow the same trend, where the β-structure is concerned, as the central NAC region displays the greatest percentage contribution to the overall peptide's character, followed by the N- and finally the C-terminal. This is in agreement with experimental observations, where the NAC region, encompassing the most hydrophobic residues, has been shown to promote protein aggregation, in contrast to the C-terminus which evidently decreases that propensity.[64]

Table 2 Secondary structure percentages from conventional MD simulations.

| Forcefield | Starting point | β character (%) | α character (%) | Other (%) |
|---|---|---|---|---|
| ff03ws (OBC) | NMR | 3.73 | 25.57 | 70.69 |
| ff03ws (OBC) | Extended | 5.68 | 24.25 | 70.06 |
| ff14SB (GBSA) | NMR | 1.63 | 47.20 | 51.17 |
| ff14SB (GBSA) | Extended | 0.12 | 40.57 | 59.31 |

Table 3 Detailed secondary structure percentages of the three main regions of αS, after conventional MD simulations.

| Region | β character (%) | α character (%) | Other (%) |
|---|---|---|---|
| | **ff03ws/OBC (NMR)** | | |
| **N-terminal** | 3.22 | 24.04 | 72.74 |
| **NAC** | 10.19 | 23.43 | 66.38 |
| **C-terminal** | 0.47 | 28.70 | 70.82 |
| | **ff03ws/OBC (extended)** | | |
| **N-terminal** | 2.75 | 24.25 | 72.99 |
| **NAC** | 20.44 | 18.19 | 61.36 |
| **C-terminal** | 0.35 | 27.88 | 71.77 |
| | **ff14SB/GBSA (NMR)** | | |
| **N-terminal** | 0.03 | 54.02 | 45.95 |
| **NAC** | 0.09 | 68.65 | 31.27 |
| **C-terminal** | 4.46 | 26.16 | 69.38 |
| | **ff14SB/GBSA (extended)** | | |
| **N-terminal** | 0.11 | 47.13 | 52.76 |
| **NAC** | 0.10 | 43.48 | 56.42 |
| **C-terminal** | 0.14 | 30.94 | 68.91 |

Table 4 $R_g$ of the peptide after conventional MD simulations.

| Forcefield | Starting point | Mean $R_g$ (Å) | SD (Å) | Max (Å) | Min (Å) |
|---|---|---|---|---|---|
| Experimental | | 40 ± 1[10] 35.5 ± 0.5[8] | | | |
| ff03ws (OBC) | NMR | 50.97 | 6.13 | 66.98 | 31.87 |
| ff03ws (OBC) | Extended | 38.80 | 3.96 | 50.90 | 26.55 |
| ff14SB (GBSA) | NMR | 20.94 | 1.05 | 24.14 | 17.99 |
| ff14SB (GBSA) | Extended | 45.53 | 4.20 | 61.57 | 31.91 |

The radius of gyration data, shown in Table 4, were compared with experimental measurements using Guinier analysis of small-angle X-ray scattering (SAXS) curve. The two references found report $R_g$ of 40 ± 1 Å,[10] and 35.5 ± 0.5 Å.[8] Starting from the extended conformation resulted in mean $R_g$ of 38.8 Å, closely resembling the mean of two experimental measurements. The systems with the NMR-

derived starting configuration, either greatly overestimate or underestimate that value, for ff03ws and ff14SB, respectively. This was expected, however, as previous studies indicate that equilibration of αS in explicit solvent requires simulations in the order of several μs to escape conformational basins.[65] The systems simulated with ff03ws, starting from both NMR-derived and extended conformations, and ff14SB with extended starting conformation, display a relatively unrestricted conformational flexibility in water, a known property of IDPs.[66] Where the ff03ws force field is concerned, although convergence to experimental values wasn't achieved with the NMR starting conformation, Figure 2, the extended peptide reached that point within the 300 ns trajectory, apparently due to the lack of bias towards any secondary structure at the outset, allowing the simulation to approach equilibrium in a reasonable timescale. The NMR-derived trajectory with ff03ws is expected to eventually arrive at the desirable values, but significantly longer simulation times would be required to leave the phase space of the starting point. The system simulated with ff14SB and started from the NMR-derived conformation results in $R_g$ values quite far from experimental values. Considering the overestimation of α-helices in this system, and how it appears to have already settled within a possible local minimum, Figure 2, the ergodicity here is not believed to improve by increasing simulation time.

Despite the disparities encountered above, from the different parameterisation of the systems, the salt bridge interactions observed in three of the four instances, Figure 8, appear in a similar pattern, with a difference on the percentages in which they appear. This is especially evident when looking at ff03ws, with the two different starting configurations. There, a similar distance between positively and negatively charged residues is observed, permitting similar electrostatic attractions to form between them, maintaining those interactions at no more than 20%. The systems simulated with the ff14SB force field, present more permanent occupancy of those interactions, even in the peptide with the extended starting conformation, which sustains the same diagonal pattern observed in the ff03ws simulations, reaching percentages as high as 43%. The peptide starting from the NMR-derived structure, and simulated with ff14SB illustrates a much more unstructured pattern in the electrostatic interactions, with occupancies reaching to values >96%, bearing further evidence of a system well confined within a local minimum.

Controversially, a similar pattern is not observed in the hydrogen bonding between the ff03ws systems and the peptide simulated from the extended conformation using ff14SB, as illustrated in Figure 9. The latter system gave significantly weaker hydrogen bonds, compared to the other three systems. The lack of off-diagonal hydrogen bonding here, hints towards a linear arrangement of the residues within the peptide, also backed by the lack of β-sheets and overestimation of α-helices. The most significant hydrogen bond interactions in each of the four cases are shown in Table S3. The

significant degree of distanced hydrogen bonds in the system simulated with ff14SB starting from NMR-derived conformation, illustrates the reason behind the greatly constrained peptide, as seen from the radius of gyration.

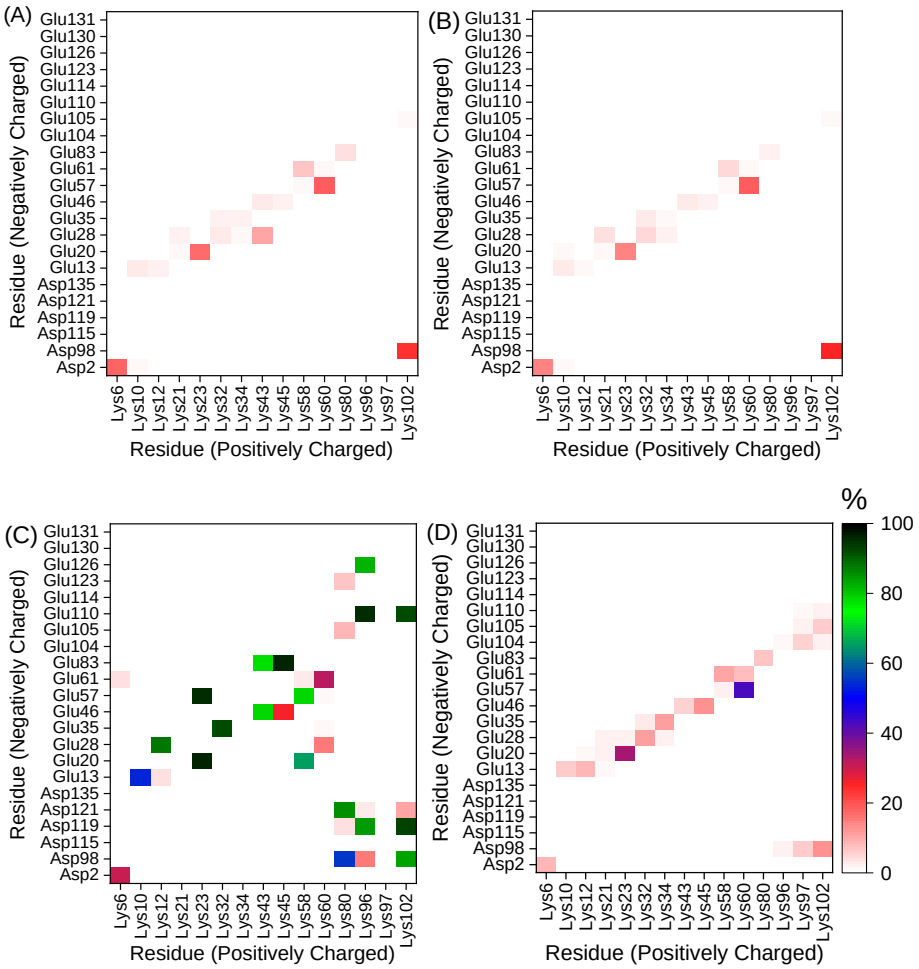


Figure 8 Salt bridges formed between negatively and positively charged residues from cMD using ff03ws with (A) NMR-defined and (B) extended starting conformations, and ff14SB with (C) NMR-defined and (D) extended starting conformations.

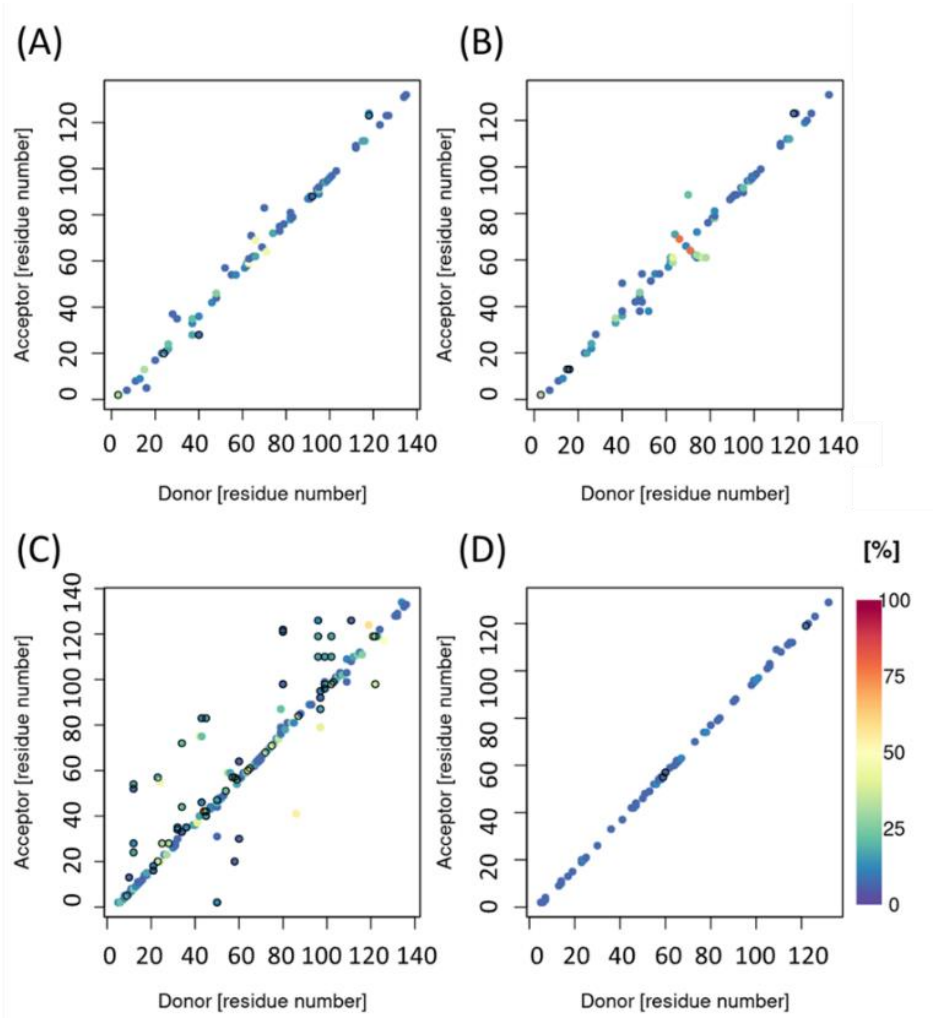


Figure 9 Hydrogen bonds present after cMD simulation, using ff03ws with (A) NMR-defined and (B) extended starting conformations and ff14SB with (C) NMR-defined and (D) extended starting conformations.

In spite of the documented performance of ff14SB/GBSA when used with more ordered peptide systems,[31] it is quite evident from the data collected here, that it is not adequate for use with αS. Considering the overestimation and difference in pattern of salt bridges, and the highly inconsistent hydrogen bond characteristics among the different starting conformations; along with the *ca.* 25 Å difference between the $R_g$ values, it is clear that ff14SB/GBSA cannot be trusted to yield an accurate trajectory in this case. On the other hand, the simulations with ff03ws/OBC have proven to be much more reliable in providing results that are both attainable, to a degree, with different starting conformations, but more importantly close to experimental findings. This particular force field has long attracted attention for use with highly disordered systems, but since its inception it has only be tested in explicit solvent systems, with a proven track record of reliable results, especially where accurate reproduction of $R_g$ is concerned, compared to other force fields.[28,53,67,68] The system that was selected to be studied further, was the one with the extended starting conformation. In order to validate

the efficiency of the implicit solvent in obtaining results with minimal loss of accuracy, the system has also been evaluated in explicit solvent.

***Explicit solvent simulations***

Having performed implicit solvent simulations on the different systems, the findings were sought to be corroborated using explicit solvent. Systems of this size, however, could not be studied starting from an extended conformation, as above, due to the very large explicit solvent box that would require, in order to permit the system to fold into a desirable conformation, without having it interact with periodic images. The computational cost such setup entails would be too great to justify. Hence, the already folded structure for the system was acquired from the final frame of conventional MD simulation in implicit solvent, and a TIP4P/2005 periodic water box was built, using LEaP,[69] around the chain at a 50 Å distance from the atoms of the solute and the solvent box edge.

The $R_g$ data illustrated in Figure S1, with a numerical account in Table 5, show a *ca.* 11 Å decrease in the size of the peptide, when simulating the peptide in explicit solvent. It is further clear that simulations in TIP4P/2005 solvent lead to much more compact conformations, than were observed either in experiment or in implicit solvent. In fact, the simulations performed in explicit solvent are so restricted that the *maximum* $R_g$ sampled is smaller than the experimental value. This shortcoming of standard water models, especially TIP3P and TIP4P, in describing αS has been noted before.[8] Even models designed specifically for IDPs, such as TIP4P-D, are found to give overly compact ensembles, which only approach experimental values after reweighting against SAXS data.[8] Nevertheless, similar studies on αS have also reported $R_g$ values within this range for explicit solvent simulations using ff03ws, as well as other force fields, with most of them giving values even less than the ones obtained with this particular force field.[67]

Table 5 $R_g$ from conventional MD simulations on the peptide in implicit and explicit solvents.

| | Mean $R_g$ (Å) | SD (Å) | Max (Å) | Min (Å) |
|---|---|---|---|---|
| ff03ws (OBC) | 38.80 | 3.96 | 50.90 | 26.55 |
| ff03ws (TIP4P/2005) | 27.56 | 4.16 | 39.01 | 19.85 |

The secondary structure characteristics of the system simulated using the explicit solvent shows a greater extent of β-sheets, with reduced α-helices, when compared to the implicit solvent simulations. A breakdown of the changes in the secondary characteristics of each of the residues, as a function of time is given in Supporting Information.

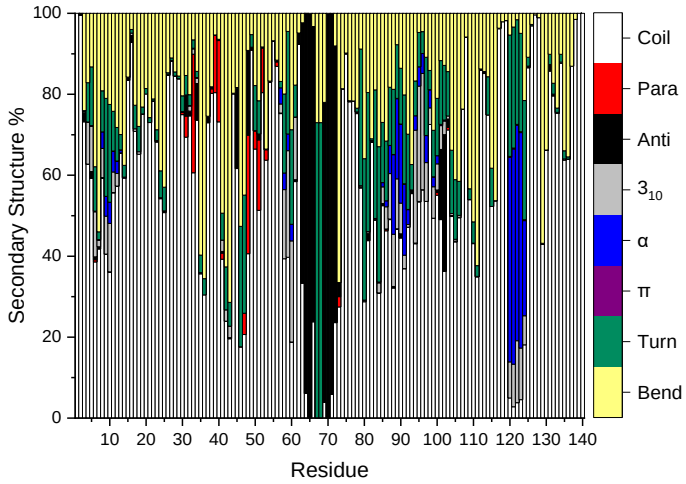


Figure 10 Secondary structure distribution per residue after cMD simulations of αS in TIP4P/2005. The β-sheets are denoted with red (parallel) and black (antiparallel), and the α-helices with grey ($3_{10}$), blue (α) and purple (π).

The contact maps of alpha carbons (Cα) and salt bridges between the residues comprising the synuclein chain are shown in Figure S4 and Figure S5, respectively. In both cases, the explicit water molecules appear to have a major effect on the interactions between formally distant residues. This comes in conflict with our previous findings on explicit solvent simulations using a smaller peptide, which did not show a large difference in the interactions found in implicit and explicit simulations.[31] The most likely culprit behind this is the effect of explicit solvent on the hydrophobic residues of the peptide, found especially in the NAC-region (residues 61-95).[70] The packing of these residues in explicit solvent, increases the rigidity of the peptide in the regions where these are found. This decrease in the flexibility of the hydrophobic residues is also illustrated in Figure S3, where in comparison to the $R_g$ of the implicit simulations, Figure S9, the NAC-region in explicit solvent appears much more restrained. The overall assessment of the above findings indicate that explicit solvent simulations do not adequately sample conformations that express structural features, such as $R_g$ and secondary structures, reported by experimental investigations,[10,15] where a more expanded peptide is reported, with α-helical values well above the *ca.* 6% occupancy observed here. Similar observations have also been reported in previous studies on α-Synuclein using ff03ws with TIP4P/2005, with the $R_g$ reported to deviate from experimental findings due either to shortcomings of the force field and solvent model or to insufficient sampling of conformations.[8,71,72]

***Conventional and Accelerated MD on αS in implicit solvent***

Having analysed conventional MD trajectories, the most promising system – ff03ws with extended starting conformation in OBC implicit solvent – was chosen to perform further calculations on. Three individual 600 ns runs were initiated, using different initial velocities, with the initial 50 ns discounted for equilibration, totalling a 1.65 μs trajectory. The final conformation in each of the runs, as well as dihedral and potential energies, were used to perform enhanced sampling simulations using accelerated MD, again using 3x600 ns runs, totalling a 1.8 μs trajectory. Below, the results from the implicit molecular dynamic simulations of αS are reported. The convergence of the system during each of the runs was evaluated by plotting RMSD as a function of simulation time (Figure 11), as well as calculating cumulative average, which settle into constant values over the course of each trajectory. The drop in RMSD values in aMD, may be attributed to the more complete convergence of the systems, considering the 600 ns initial NVT dynamics performed on each of the repeats. $R_g$ values over cMD and the aMD trajectories, are shown in Figure 12, along with the cumulative average. The rolling standard deviation (with a 25 ns window) of the simulations were also plotted, Figure S7, change of SD over time, providing further evidence of equilibration over the course of each run. From these plots, it is evident that the system fluctuates between a range of $R_g$ values, with a mean SD of cMD: 4.28 Å and aMD: 4.55 Å.

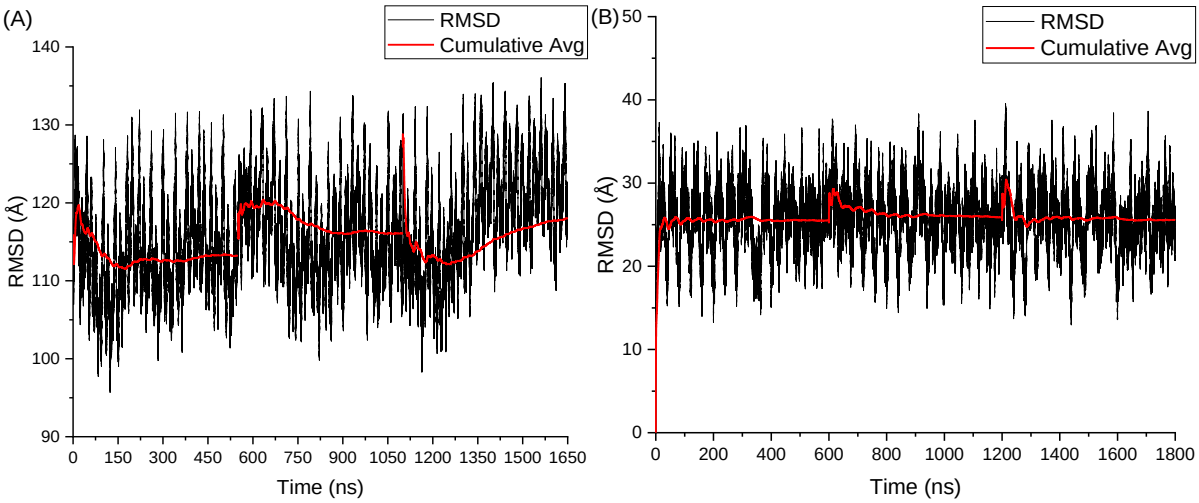


Figure 11 RMSD plots of (A) conventional and (B) accelerated MD of αS, with the cumulative average shown in red.

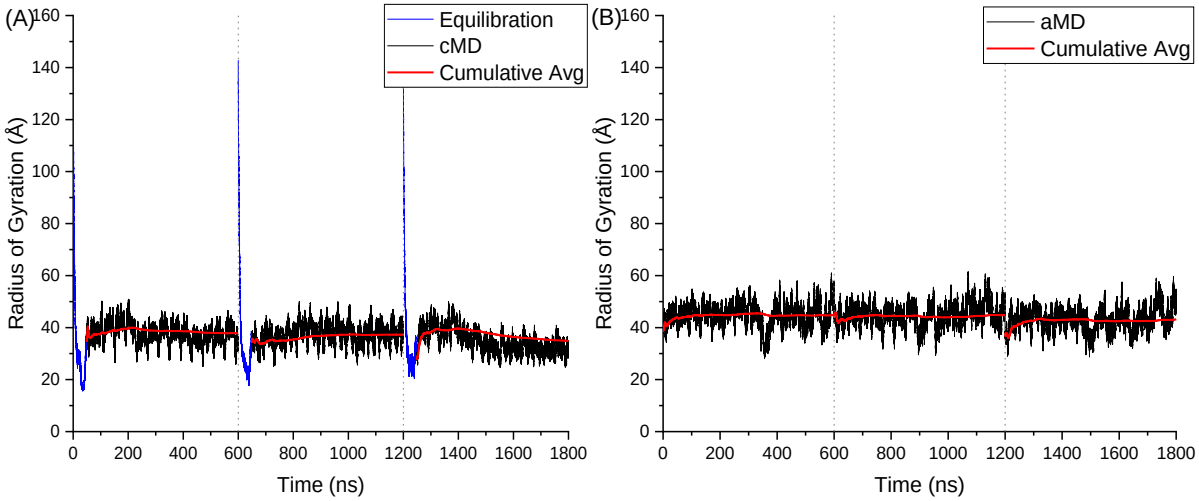

Figure 12 Radius of gyration plot, showing the (A) change from equilibration to cMD and (B) aMD simulations, with the cumulative average shown in red.

Table 6 $R_g$ from conventional and accelerated MD simulations.

| | Mean $R_g$ (Å) | SD (Å) | Max (Å) | Min (Å) |
|---|---|---|---|---|
| Experimental | 40 ± 1 Å,[10] 35.5 ± 0.5 Å[8] | | | |
| conventional MD | 36.65 | 4.28 | 50.90 | 24.67 |
| accelerated MD | 44.26 | 4.58 | 61.50 | 28.07 |

Looking at the $R_g$ value from the conventional MD simulations of the aggregate 1.65 μs trajectory, a thing of note is the increase in compactness by just *ca.* 2 Å, when compared to the initial 300 ns cMD trajectory, suggesting that Rg was already close to convergence within that timeframe. Upon comparison of data from conventional to accelerated MD, an overall decrease in the compactness of the peptide may be observed. This comes as a result of the extended conformational space explored by the aMD, visiting conformations with $R_g$ as high as 62 Å, in contrast to those explored by cMD, which reach 51 Å. The secondary structure characteristics of the aMD trajectory decrease by quite a significant degree compared to conventional MD, owing to the increased range of conformations sampled using this method. Nevertheless, the ratio of β-characteristics in the different regions of the peptide remains relatively consistent with observations made in the conventional MD, with the highest percentage of sheets present in the NAC region, followed by the N- and C-termini. The secondary structure characteristics of the peptide are shown in Figure 14, Table 7 and Table 8. The NAC region of the peptide has long been thought to be directly involved in the pathogenesis of PD, owing to the formation a hydrophobic β-sheet intermediate in that particular region.[73] This structure appears predominantly in the conventional dynamics, possibly owing to the lack of the added bias

potential, permitting the sustainment of a more stable conformation. The lack of overestimation of secondary characteristics in the accelerated MD trajectories, is ascribed to the added boost, pushing the simulations out of meta-stable local minima. The conventional MD simulations should also, in principle, break away from such minima, but in practise they often do not in the timescales used here.

As noted earlier, one of the greatest contribution of β-characteristics in the systems is the β-hairpin regions, populating around KTK(E/Q)GV repeats (between residues 21-26, 32-37 and 43-48), up to KTKEQV (residues 58-63), as well as the region between residues 63-72. The presence of these secondary structures, may be seen from Figure S8, with an illustration in Figure 13. Looking at Figure 14, there is an increase in the fluctuation of the residues in the NAC region going from conventional to accelerated MD, as a result of the significant β-hairpin region, dominating the secondary characteristics in conventional MD.

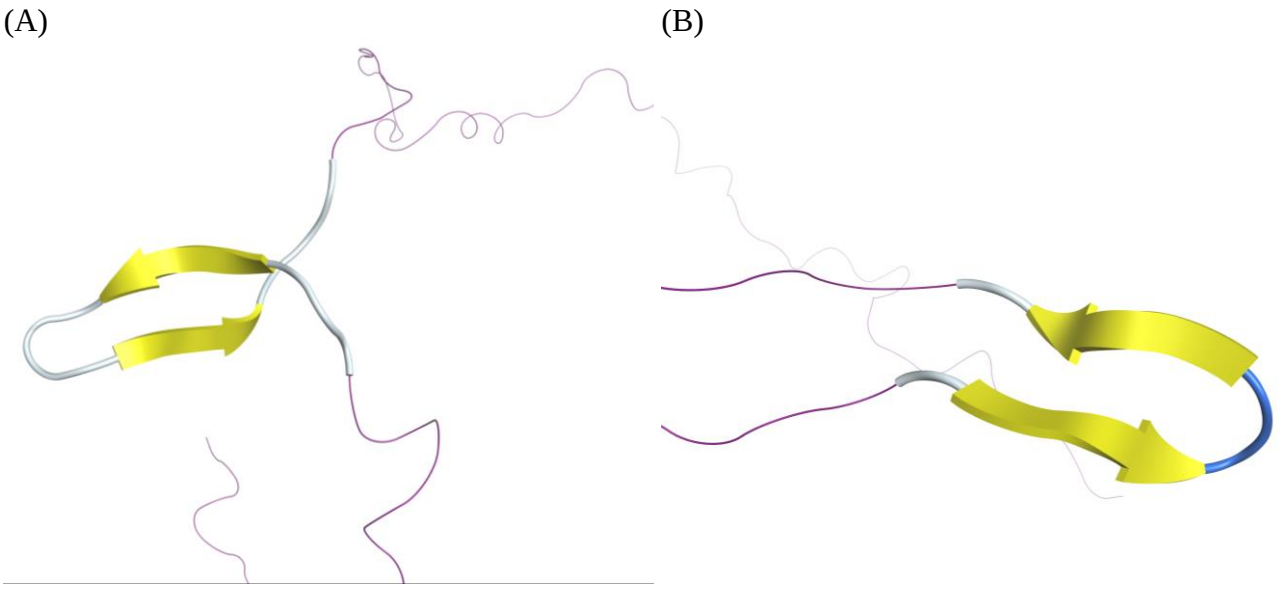


Figure 13 β-hairpin structure found between (A) residues 38-53 and (B) 63-72.

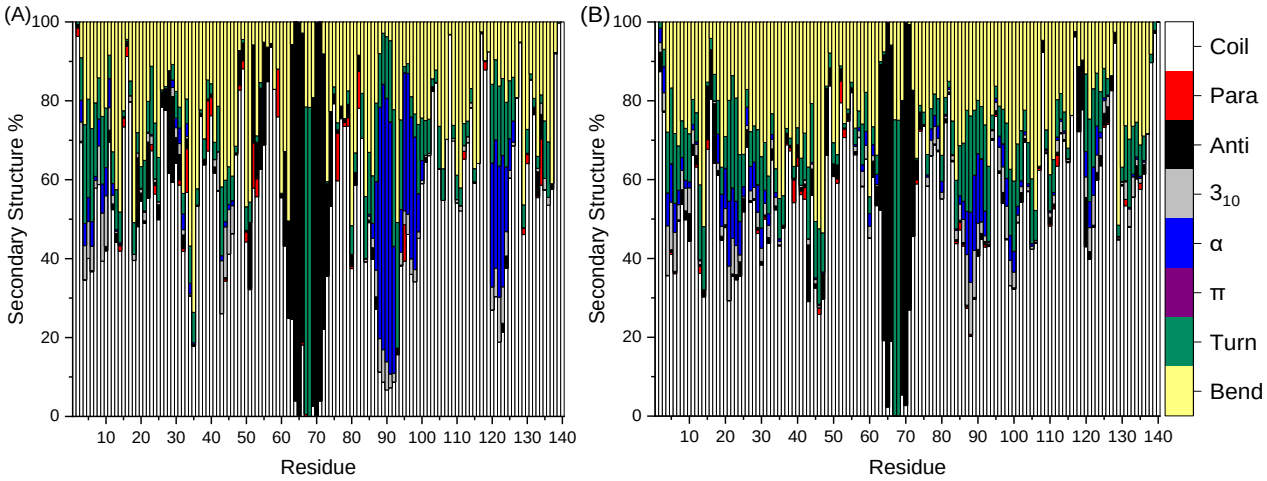


Figure 14 Secondary structure distribution per residue after (A) 1.65 μs cMD and (B) 1.80 μs aMD of αS, using ff03ws with extended starting conformation. The β-sheets are denoted with red (parallel) and black (antiparallel), and the α-helices with grey ($3_{10}$), blue (α) and purple (π).

Table 7 Detailed secondary structure percentages of the three main regions of αS, after c/aMD simulations using ff03ws.

| **Region** | **β character (%)** | **α character (%)** | **Other (%)** |
|---|---|---|---|
| | **conventional MD** | | |
| **N-terminal** | 7.35 | 21.44 | 71.21 |
| **NAC** | 15.67 | 15.73 | 68.60 |
| **C-terminal** | 0.33 | 28.08 | 71.59 |
| | **accelerated MD** | | |
| **N-terminal** | 2.12 | 16.30 | 81.58 |
| **NAC** | 6.84 | 14.56 | 78.61 |
| **C-terminal** | 0.26 | 18.05 | 81.69 |

Table 8 Secondary structure percentages for the peptide after conventional and accelerated MD simulations in implicit solvent.

| | β character (%) | α character (%) | Other (%) |
|---|---|---|---|
| conventional MD | 6.63 | 22.59 | 70.79 |
| accelerated MD | 2.47 | 16.55 | 80.98 |

Predicted Cα chemical shifts further substantiate the effectiveness of the ff03ws/OBC combination in providing results that reflect experimental findings. The *ca.* 1200 frames extracted from the total 165,000 and 180,000 frame trajectories, by sampling every 137$^{th}$ and 150$^{th}$ frame, from the conventional and accelerated MD simulations, respectively, present a further decrease in the percentage error from the experimental values,[60] reported in the evaluation of the starting conformation above; as well as coming close to the values from the simulations in explicit solvent (mean error: 1.58%, Table S2) using conventional MD, and surpassing them with the accelerated MD

simulations. The mean errors from the cMD and aMD frame excerpts, are 1.89% and 1.42%, respectively. Below, Figure 15 illustrates the close resemblance of the chemical shifts from the accelerated MD simulations to experimental values, diminishing the error from the three main regions of the peptide, to 1.26% for the NAC region, 1.35% and 1.63% for the N- and C-termini, respectively.

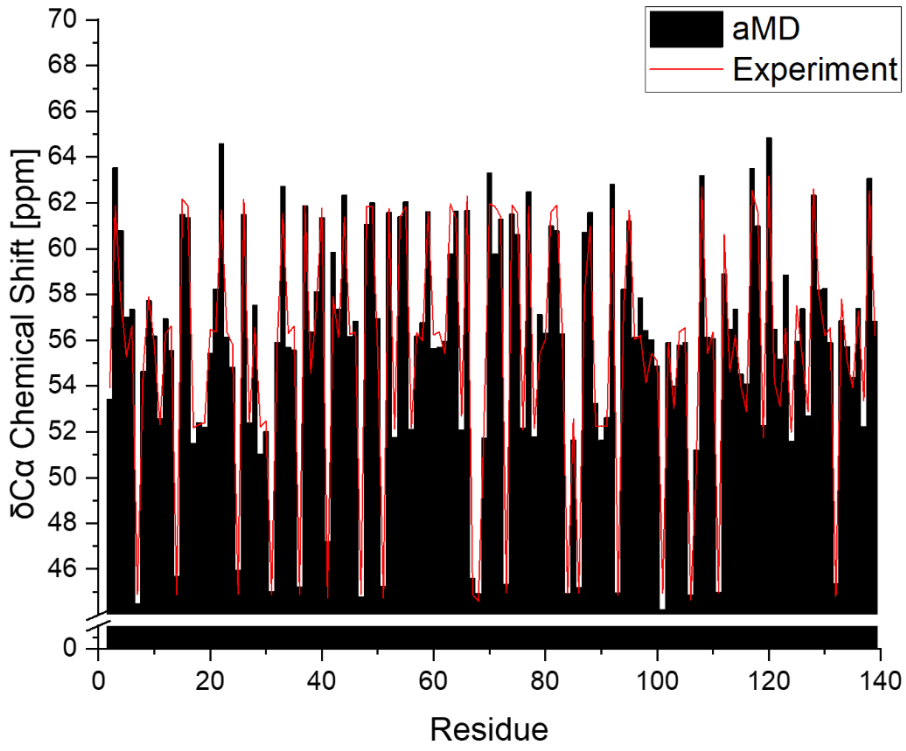


Figure 15 Predicted Cα chemical shift values per residue, from 1200 frames taken from the conventional and accelerated MD simulations on αS (black). Experimental data (red) obtained from source.[60]

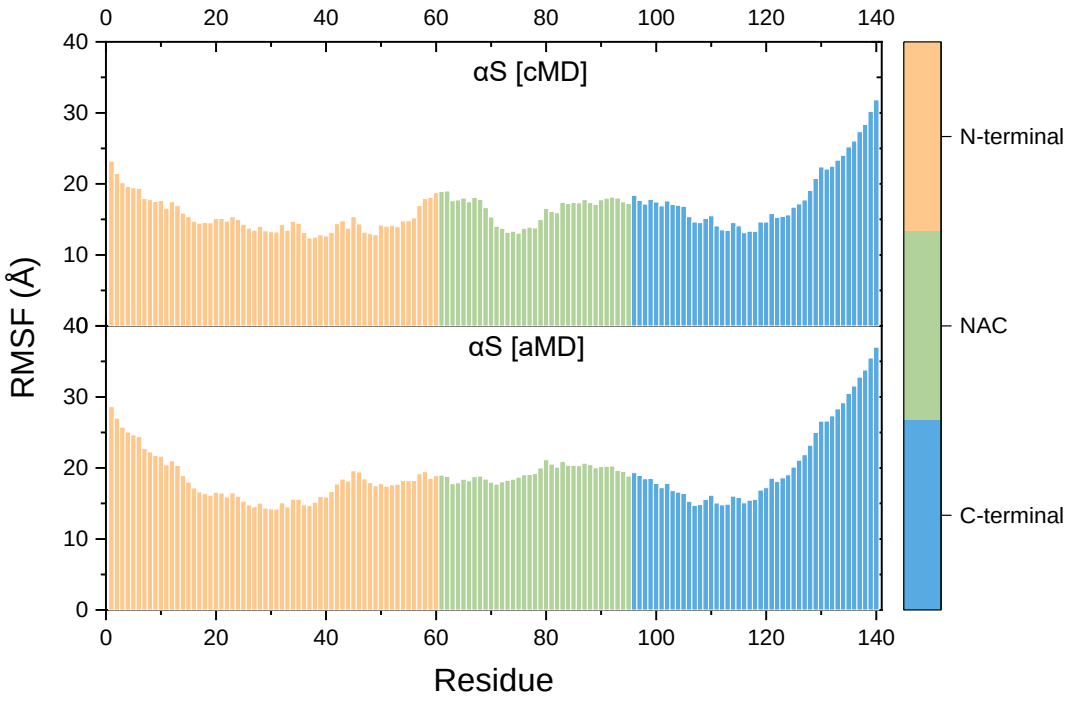

Figure 16 Root mean square fluctuation of individual residues from conventional and accelerated MD

Looking at the intramolecular interactions of the peptide, there are differences, depending on the simulation method employed. The RMSF plot, Figure 16, illustrates a more flexible system in the accelerated MD simulations, particularly in the two termini, but also in the NAC region, around residues 65-80. The increase in flexibility in that region can be attributed to the breakage of the quite sustained β-hairpin structure seen in conventional MD, between residues 63-72. The salt bridges, alpha C contact maps and hydrogen bonds, Figure 17 Figure 18 and Figure 19, respectively, maintain most of the characteristic interactions, between the two methods. The only apparent difference being the off-diagonal interactions that are expressed in the conventional MD trajectory. The absence of similar features in the accelerated MD, could be attributed to the added bias, driving the system to explore other conformations, without settling into energy wells. Reflecting on the data collected above, the superior method is believed to be the accelerated MD methodology, that introduces boost potential into the system, increasing the inherent flexibility of the peptide, permitting the trajectory to sample more varied conformations in phase space.

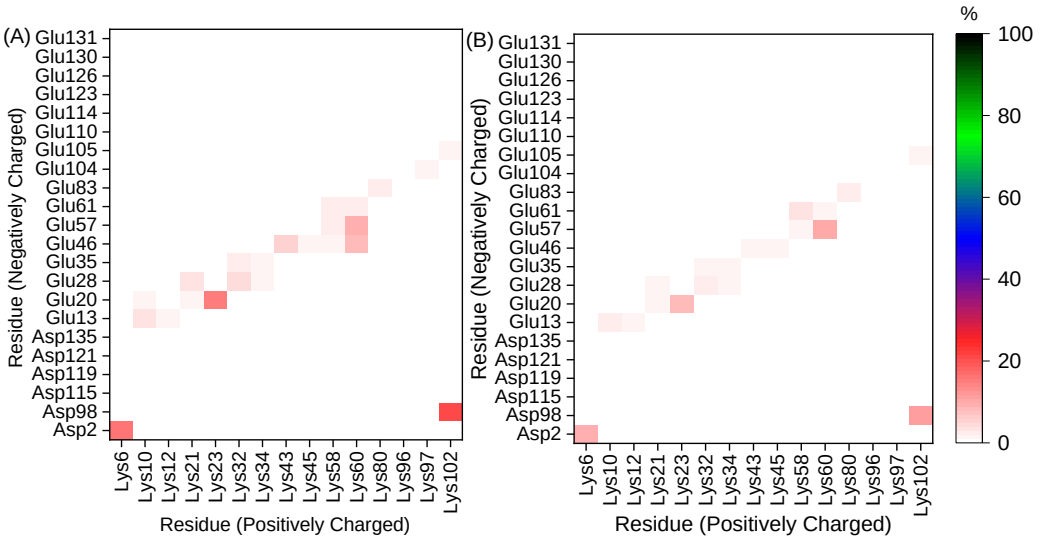


Figure 17 Salt bridges formed between negatively and positively charged residues from (A) conventional and (B) accelerated MD simulations.

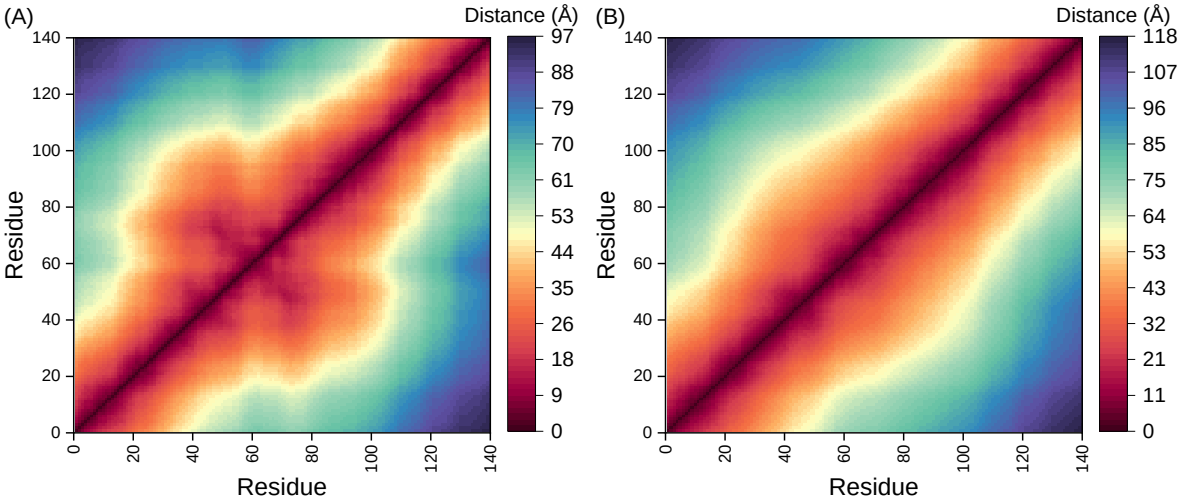


Figure 18 Contact maps of the alpha-C from (A) conventional and (B) accelerated MD simulations.

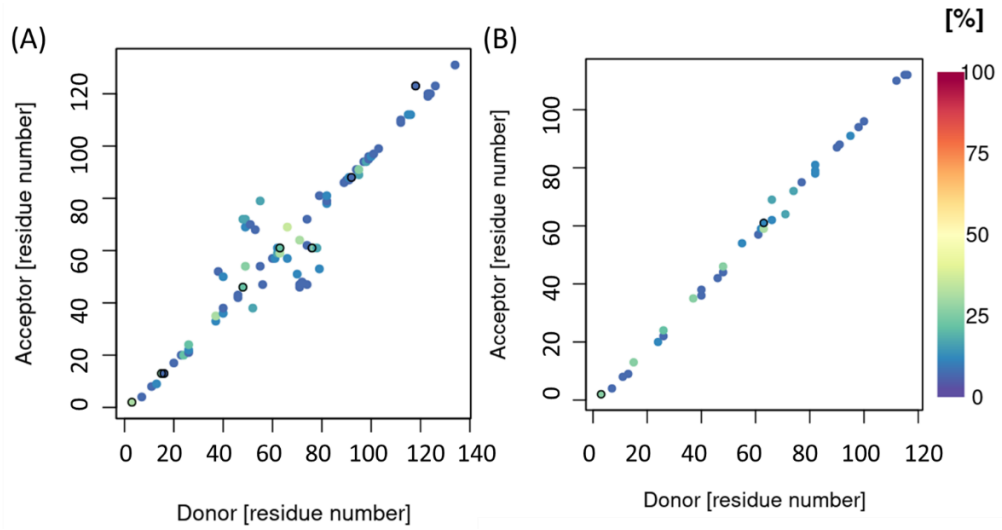


Figure 19 Hydrogen bonds present after (A) conventional and (B) accelerated MD simulations.

The free energy landscape plot of end-to-end distance against $R_g$, illustrate the conformational space explored by the system, reaching an end-to-end distance up to 210 Å, and $R_g$ values ranging between 25-65 Å, with lowest PMF values reached at *ca*. $R_g$ 40-45 Å and end-to-end distance 100-140 Å. The reweighted secondary characteristics, Figure 21, give a detailed breakdown of the different percentages of each of the structures, explored throughout the sampled conformational space. The greatest β-character is predominantly expressed between $R_g$ 28-52 Å, where it fluctuates between 0-10%, reaching up to values of 20%. The α-helical characteristics of the peptide extend up to 48% at various $R_g$ values between 34-54 Å, with most of the time spent between 10-20% regardless of the $R_g$ value.

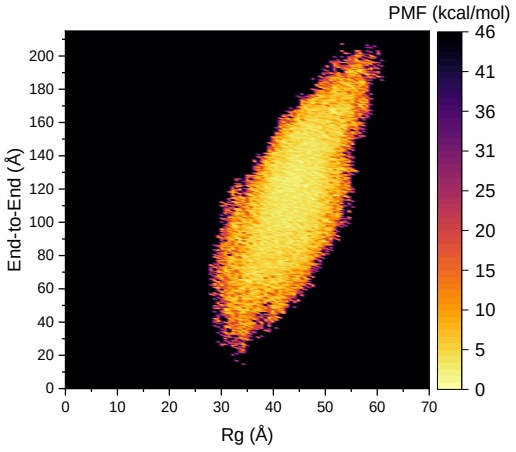


Figure 20 2D free energy plot (FEP) of the end-to-end distance against the radius of gyration ($R_g$), from the aMD simulations.

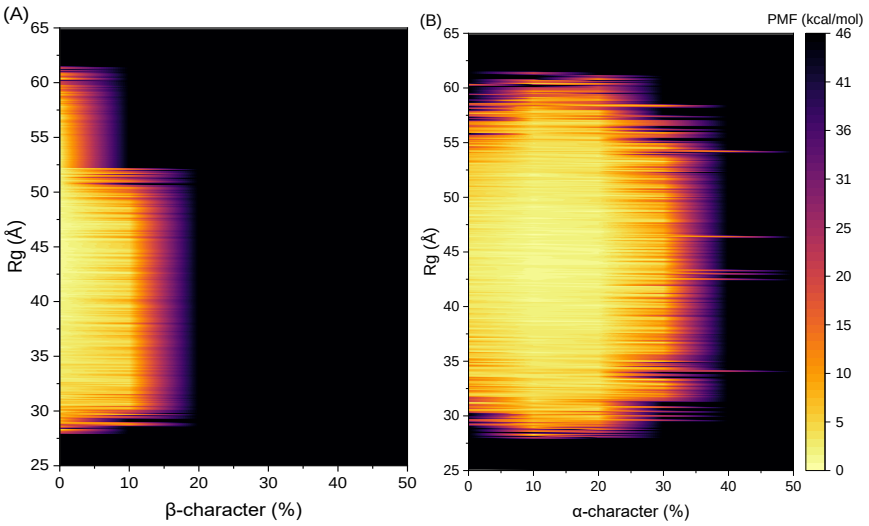


Figure 21 2D free energy plot (FEP) of the radius of gyration ($R_g$) against the percentage (A) β- and (B) α-secondary structure, from the aMD simulations.

## Conclusions

Herein we report conventional and accelerated MD simulations on α-Synuclein, using implicit and explicit water models, as well as evaluating the force field and starting conformation of the simulations. We show that the ff03ws forcefield with OBC implicit solvent model reproduces key structural features of the isolated peptide, approaching the mean $R_g$ obtained from SAXS studies and the overall percentages of secondary structural characteristics. We also show that accelerated MD provide significantly greater sampling of the ensemble of conformations available to αS. This method is found to deliver values close to experimental observations more consistently when compared to conventional MD, owing to the introduction of a bias in the potential and dihedral energies of the system, permitting the exploration of a greater conformational space.

An evaluation of the backbone and sidechain C chemical shifts, against experimental data, corroborates the validity of the force field and solvent combination employed herein, particularly when accelerated MD simulations were used with the ff03ws/OBC, resulting in a mean % error of the predicted Cα chemical shifts, against the reported experimental chemical shifts,[60] to 1.42%. Concurrently, also making the case for how the mean secondary structure percentages are better broken down to individual regions for a better function-related assessment. The key motifs reported throughout the literature, between residues 38-53, have further been used to validate the suitability of the reported MM methodology used here. Analysis of aMD trajectories, encompassing radius of gyration, RMSF and secondary structure, provide evidence of an average decrease in the perpetuity of the characteristics expressed in the conventional MD simulations, as a result of the increased conformational space visited in the former case. This is a result of the bias in the potential energy

pushing the system out of conformational basins, permitting the sampling of a more expanded assortment of features. The free-energy landscape plots, from the accelerated MD simulations, highlight the variety of secondary structure percentages surveyed in the trajectory at different $R_g$ values, falling well within the percentages reported from experimental studies, using CD, and Raman and ATR-FTIR spectroscopic techniques.

The results we present also give clear evidence of the advantages of implicit solvent over the explicit water model in the simulation of the dynamics of α-Synuclein, with the latter resulting in a compact and rigid conformational assembly of the peptide chain. This may be attributed to the extensive presence of hydrophobic residues in α-Synuclein, resulting in an increase rigidity of such residues when simulated around explicit solvent. The structural arrangement of the backbone of the peptide from the implicit solvent simulations come in close agreement with experimental values, when simulated with the accelerated MD methodology, accentuating how the length and repeats of the simulations carried out here, produce a reliable representation of the mean representative structures seen in the referenced studies. Taken together, our results indicate that the dynamical behaviour of α-Synuclein can be reliably studied using suitable choice of forcefield and implicit solvent model.

**Acknowledgements**

We acknowledge the role of Advanced Research Computing @ Cardiff (ARCCA) in providing computational resources for simulations.

**References**

1 K. Ueda, H. Fukushima, E. Masliah, Y. U. Xia, A. Iwai, M. Yoshimoto, D. A. C. Otero, J. Kondo, Y. Ihara and T. Saitoh, Molecular cloning of cDNA encoding an unrecognized component of amyloid in Alzheimer disease, *Proc. Natl. Acad. Sci. USA*, 1993, **90**, 11282–11286.

2 V. N. Uversky, Unusual biophysics of intrinsically disordered proteins, *Biochim. Biophys. Acta - Proteins Proteomics*, 2013, **1834**, 932–951.

3 C. J. Oldfield and A. K. Dunker, Intrinsically disordered proteins and intrinsically disordered protein regions, *Annu. Rev. Biochem.*, 2014, **83**, 553–584.

4 J. A. Rodriguez, M. I. Ivanova, M. R. Sawaya, D. Cascio, F. E. Reyes, D. Shi, S. Sangwan, E. L. Guenther, L. M. Johnson, M. Zhang, L. Jiang, M. A. Arbing, B. L. Nannenga, J. Hattne, J. Whitelegge, A. S. Brewster, M. Messerschmidt, S. Boutet, N. K. Sauter, T. Gonen and D. S. Eisenberg, Structure of the toxic core of α-synuclein from invisible crystals, *Nature*, 2015, **525**, 486–490.

5 R. M. Meade, D. P. Fairlie and J. M. Mason, Alpha-synuclein structure and Parkinson's disease, *Mol. Neurodegener.*, 2019, **14**, 1–14.

6 D. Eliezer, E. Kutluay, R. Bussell and G. Browne, Conformational properties of α-synuclein in its free and lipid-associated states, *J. Mol. Biol.*, 2001, **307**, 1061–1073.

7 M. D. Tuttle, G. Comellas, A. J. Nieuwkoop, D. J. Covell, D. A. Berthold, K. D. Kloepper, J. M. Courtney, J. K. Kim, A. M. Barclay, A. Kendall, W. Wan, G. Stubbs, C. D. Schwieters, V. M. Y. Lee, J. M. George and C. M. Rienstra, Solid-state NMR structure of a pathogenic fibril of full-length human α-synuclein, *Nat. Struct. Mol. Biol.*, 2016, **23**, 409–415.

8 M. C. Ahmed, L. K. Skaanning, A. Jussupow, E. A. Newcombe, B. B. Kragelund, C. Camilloni, A. E. Langkilde and K. Lindorff-Larsen, Refinement of α-Synuclein Ensembles Against SAXS Data: Comparison of Force Fields and Methods, *Front. Mol. Biosci.*, 2021, **8**, 1–13.

9 V. N. Uversky, E. M. Cooper, K. S. Bower, J. Li and A. L. Fink, Accelerated α-synuclein fibrillation in crowded milieu, *FEBS Lett.*, 2002, **515**, 99–103.

10 V. N. Uversky, J. Li and A. L. Fink, Evidence for a Partially Folded Intermediate in α-Synuclein Fibril Formation, *J. Biol. Chem.*, 2001, **276**, 10737–10744.

11 A. Rekas, R. B. Knott, A. Sokolova, K. J. Barnham, K. A. Perez, C. L. Masters, S. C. Drew, R. Cappai, C. C. Curtain and C. L. L. Pham, The structure of dopamine induced α-synuclein oligomers, *Eur. Biophys. J.*, 2010, **39**, 1407–1419.

12 X.-J. Lin, F. Zhang, Y.-Y. Xie, W.-J. Bao, J.-H. He and H.-Y. Hu, Secondary structural formation of α-synuclein amyloids as revealed byg-factor of solid-state circular dichroism, *Biopolymers*, 2006, **83**, 226–232.

13 J. Burré, S. Vivona, J. Diao, M. Sharma, A. T. Brunger and T. C. Südhof, Properties of native brain α-synuclein, *Nature*, 2013, **498**, 107–110.

14 N. P. Ulrih, C. H. Barry and A. L. Fink, Impact of Tyr to Ala mutations on α-synuclein fibrillation and structural properties, *Biochim. Biophys. Acta - Mol. Basis Dis.*, 2008, **1782**, 581–585.

15 M. M. Apetri, N. C. Maiti, M. G. Zagorski, P. R. Carey and V. E. Anderson, Secondary Structure of a -Synuclein Oligomers : Characterization by Raman and Atomic Force Microscopy, 2006, 63–71.

16 N. C. Maiti, M. M. Apetri, M. G. Zagorski, P. R. Carey and V. E. Anderson, Raman Spectroscopic Characterization of Secondary Structure in Natively Unfolded Proteins: α-Synuclein, *J. Am. Chem. Soc.*, 2004, **126**, 2399–2408.

17 B. A. Silva, Ó. Einarsdóttir, A. L. Fink and V. N. Uversky, Biophysical characterization of α-synuclein and rotenone interaction, *Biomolecules*, 2013, **3**, 703–732.

18 A. L. Mahul-Mellier, J. Burtscher, N. Maharjan, L. Weerens, M. Croisier, F. Kuttler, M. Leleu, G. W. Knott and H. A. Lashuel, The process of Lewy body formation, rather than simply α-synuclein fibrillization, is one of the major drivers of neurodegeneration, *Proc. Natl. Acad. Sci. U. S. A.*, 2020, **117**, 4971–4982.

19 L. Xu, R. Nussinov and B. Ma, Coupling of the non-amyloid-component (NAC) domain and the KTK(E/Q)GV repeats stabilize the α-synuclein fibrils, *Eur. J. Med. Chem.*, 2016, **121**, 841–850.

20 D. E. Mor, S. E. Ugras, M. J. Daniels and H. Ischiropoulos, Dynamic structural flexibility of α-synuclein, *Neurobiol. Dis.*, 2016, **88**, 66–74.

21 S. Y. Mandaci, M. Caliskan, M. F. Sariaslan, V. N. Uversky and O. Coskuner-Weber, Epitope region identification challenges of intrinsically disordered proteins in neurodegenerative diseases: Secondary structure dependence of α-synuclein on simulation techniques and force field parameters, *Chem. Biol. Drug Des.*, 2020, **96**, 659–667.

22 R. Ramis, J. Ortega-Castro, B. Vilanova, M. Adrover and J. Frau, Cu2+, Ca2+, and methionine oxidation expose the hydrophobic α-synuclein NAC domain, *Int. J. Biol. Macromol.*, 2021, **169**, 251–263.

23 T. S. Choi, J. Lee, J. Y. Han, B. C. Jung, P. Wongkongkathep, J. A. Loo, M. J. Lee and H. I. Kim, Supramolecular Modulation of Structural Polymorphism in Pathogenic α-Synuclein Fibrils Using Copper(II) Coordination, *Angew. Chemie - Int. Ed.*, 2018, **57**, 3099–3103.

24 F. Rose, M. Hodak and J. Bernholc, Mechanism of copper(II)-induced misfolding of Parkinson's disease protein, *Sci. Rep.*, 2011, **1**, 1–5.

25 O. C. Weber and V. N. Uversky, How accurate are your simulations? Effects of confined aqueous volume and AMBER FF99SB and CHARMM22/CMAP force field parameters on structural ensembles of intrinsically disordered proteins: Amyloid-β 42 in water , *Intrinsically Disord. Proteins*, 2017, **5**, e1377813.

26 O. Coskuner and O. Wise-Scira, Structures and free energy landscapes of the A53T mutant-type α-synuclein protein and impact of A53T mutation on the structures of the wild-type α-synuclein protein with dynamics, *ACS Chem. Neurosci.*, 2013, **4**, 1101–1113.

27 A. Sanjeev and V. Kumar Mattaparthi, Computational Investigation on Tyrosine to Alanine Mutations Delaying the Early Stage of α-Synuclein Aggregation, *Curr. Proteomics*, 2017, **14**, 31–41.

28 R. B. Best, W. Zheng and J. Mittal, Balanced protein-water interactions improve properties of disordered proteins and non-specific protein association, *J. Chem. Theory Comput.*, 2014, **10**, 5113–5124.

29 D. Song, R. Luo and H.-F. Chen, The IDP-Specific Force Field ff14IDPSFF Improves the

Conformer Sampling of Intrinsically Disordered Proteins, *J. Chem. Inf. Model.*, 2017, **57**, 1166–1178.

30 D. A. Case, R. M. Betz, D. S. Cerutti, T. E. Cheatham, T. A. Darden, R. E. Duke, T. J. Giese, H. Gohlke, A. W. Goetz, N. Homeyer, S. Izadi, P. Janowski, J. Kaus, A. Kovalenko, T. S. Lee, S. LeGrand, P. Li, C. Lin, T. Luchko, R. Luo, B. Madej, D. Mermelstein, K. M. Merz, G. Monard, H. Nguyen, H. T. Nguyen, I. Omelyan, A. Onufriev, D. R. Roe, A. Roitberg, C. Sagui, C. L. Simmerling, W. M. Botello-Smith, J. Swails, R. C. Walker, J. Wang, R. M. Wolf, X. Wu, L. Xiao and P. A. Kollman, *AMBER 2016*, San Francisco, 2016.

31 N. Al-Shammari, L. Savva, O. Kennedy-Britten and J. A. Platts, Forcefield evaluation and accelerated molecular dynamics simulation of Zn(II) binding to N-terminus of amyloid-β, *Comput. Biol. Chem.*, 2021, **93**, 107540.

32 T. J. Dick and J. D. Madura, Chapter 5 A Review of the TIP4P, TIP4P-Ew, TIP5P, and TIP5P-E Water Models, *Annu. Rep. Comput. Chem.*, 2005, **1**, 59–74.

33 G. D. Hawkins, C. J. Cramer and D. G. Truhlar, Pairwise solute descreening of solute charges from a dielectric medium, *Chem. Phys. Lett.*, 1995, **246**, 122–129.

34 G. D. Hawkins, C. J. Cramer and D. G. Truhlar, Parametrized Models of Aqueous Free Energies of Solvation Based on Pairwise Descreening of Solute Atomic Charges from a Dielectric Medium, *J. Phys. Chem.*, 1996, **100**, 19824–19839.

35 A. Onufriev, D. Bashford and D. A. Case, Modification of the generalized born model suitable for macromolecules, *J. Phys. Chem. B*, 2000, **104**, 3712–3720.

36 U. R. Shrestha, P. Juneja, Q. Zhang, V. Gurumoorthy, J. M. Borreguero, V. Urban, X. Cheng, S. V. Pingali, J. C. Smith, H. M. O'Neill and L. Petridis, Generation of the configurational ensemble of an intrinsically disordered protein from unbiased molecular dynamics simulation, *Proc. Natl. Acad. Sci. U. S. A.*, 2019, **116**, 20446–20452.

37 W. Zheng, A. Borgia, K. Buholzer, A. Grishaev, B. Schuler and R. B. Best, Probing the Action of Chemical Denaturant on an Intrinsically Disordered Protein by Simulation and Experiment, *J. Am. Chem. Soc.*, 2016, **138**, 11702–11713.

38 M. M. J. Bellaiche and R. B. Best, Molecular Determinants of Aβ42 Adsorption to Amyloid Fibril Surfaces, *J. Phys. Chem. Lett.*, 2018, **9**, 6437–6443.

39 Y. Duan, C. Wu, S. Chowdhury, M. C. Lee, G. Xiong, W. Zhang, R. Yang, P. Cieplak, R. Luo, T. Lee, J. Caldwell, J. Wang and P. Kollman, A point-charge force field for molecular mechanics simulations of proteins based on condensed-phase quantum mechanical calculations, *J. Comput. Chem.*, 2003, **24**, 1999–2012.

40 V. A. Voelz, K. A. Dill and I. Chorny, Peptoid conformational free energy landscapes from implicit-solvent molecular simulations in AMBER., *Biopolymers*, 2011, **96**, 639–650.

41 S. Patel, V. Ramanujam, A. K. Srivastava and K. V. R. Chary, Conformational propensities and dynamics of a βγ-crystallin, an intrinsically disordered protein, *Phys. Chem. Chem. Phys.*, 2014, **16**, 12703–12718.

42 M. S. Shell, R. Ritterson and K. A. Dill, A test on peptide stability of AMBER force fields with implicit solvation, *J. Phys. Chem. B*, 2008, **112**, 6878–6886.

43 H. Lei, C. Wu, Z.-X. Wang, Y. Zhou and Y. Duan, Folding processes of the B domain of protein A to the native state observed in all-atom ab initio folding simulations, *J. Chem. Phys.*, 2008, **128**, 235105.

44 C. Rungnim, T. Rungrotmongkol, S. Hannongbua and H. Okumura, Replica exchange molecular dynamics simulation of chitosan for drug delivery system based on carbon nanotube, *J. Mol. Graph. Model.*, 2013, **39**, 183–192.

45 L. Gallego-Villar, C. Pérez-Cerdá, B. Pérez, D. Abia, M. Ugarte, E. Richard and L. R. Desviat, Functional characterization of novel genotypes and cellular oxidative stress studies in propionic acidemia, *J. Inherit. Metab. Dis.*, 2013, **36**, 731–740.

46 T. S. Ulmer, A. Bax, N. B. Cole and R. L. Nussbaum, Structure and dynamics of micelle-bound human α-synuclein, *J. Biol. Chem.*, 2005, **280**, 9595–9603.

47 R. J. Deeth, N. Fey and B. Williams-Hubbard, DommiMOE: An implementation of ligand field molecular mechanics in the molecular operating environment, *J. Comput. Chem.*, 2005, **26**, 123–130.

48 J. A. Izaguirre, D. P. Catarello, J. M. Wozniak and R. D. Skeel, Langevin stabilization of molecular dynamics, *J. Chem. Phys.*, 2001, **114**, 2090–2098.

49 V. Kräutler and W. F. V. A. N. Gunsteren, A Fast SHAKE Algorithm to Solve Distance Constraint Equations for Small Molecules in Molecular, 2001, **22**, 501–508.

50 A. K. Somavarapu and K. P. Kepp, The Dependence of Amyloid-β Dynamics on Protein Force Fields and Water Models, *ChemPhysChem*, 2015, **16**, 3278–3289.

51 S. Bhattacharya, L. Xu and D. Thompson, Molecular Simulations Reveal Terminal Group Mediated Stabilization of Helical Conformers in Both Amyloid-β42 and α-Synuclein, *ACS Chem. Neurosci.*, 2019, **10**, 2830–2842.

52 R. Ramis, J. Ortega-Castro, R. Casasnovas, L. Marino, B. Vilanova, M. Adrover and J. Frau, A Coarse-Grained Molecular Dynamics Approach to the Study of the Intrinsically Disordered Protein α-Synuclein, *J. Chem. Inf. Model.*, 2019, **59**, 1458–1471.

53 S. Rauscher, V. Gapsys, M. J. Gajda, M. Zweckstetter, B. L. de Groot and H. Grubmüller, Structural Ensembles of Intrinsically Disordered Proteins Depend Strongly on Force Field: A Comparison to Experiment, *J. Chem. Theory Comput.*, 2015, **11**, 5513–5524.

54 M. Chan-Yao-Chong, D. Durand and T. Ha-Duong, Molecular Dynamics Simulations

Combined with Nuclear Magnetic Resonance and/or Small-Angle X-ray Scattering Data for Characterizing Intrinsically Disordered Protein Conformational Ensembles, *J. Chem. Inf. Model.*, 2019, **59**, 1743–1758.

55 O. Coskuner-Weber and V. Uversky, Insights into the Molecular Mechanisms of Alzheimer's and Parkinson's Diseases with Molecular Simulations: Understanding the Roles of Artificial and Pathological Missense Mutations in Intrinsically Disordered Proteins Related to Pathology, *Int. J. Mol. Sci.*, 2018, **19**, 336.

56 Y. Miao, W. Sinko, L. Pierce, D. Bucher, R. C. Walker and J. A. McCammon, Improved reweighting of accelerated molecular dynamics simulations for free energy calculation, *J. Chem. Theory Comput.*, 2014, **10**, 2677–2689.

57 D. R. Roe and T. E. Cheatham, PTRAJ and CPPTRAJ: Software for processing and analysis of molecular dynamics trajectory data, *J. Chem. Theory Comput.*, 2013, **9**, 3084–3095.

58 Y. Cai, C. Lendel, L. Österlund, A. Kasrayan, L. Lannfelt, M. Ingelsson, F. Nikolajeff, M. Karlsson and J. Bergström, Changes in secondary structure of α-synuclein during oligomerization induced by reactive aldehydes, *Biochem. Biophys. Res. Commun.*, 2015, **464**, 336–341.

59 Y. Shen and A. Bax, SPARTA+: A modest improvement in empirical NMR chemical shift prediction by means of an artificial neural network, *J. Biomol. NMR*, 2010, **48**, 13–22.

60 W. Bermel, I. Bertini, I. C. Felli, Y. M. Lee, C. Luchinat and R. Pierattelli, Protonless NMR experiments for sequence-specific assignment of backbone nuclei in unfolded proteins, *J. Am. Chem. Soc.*, 2006, **128**, 3918–3919.

61 J. A. Marsh, V. K. Singh, Z. Jia and J. D. Forman-Kay, Sensitivity of secondary structure propensities to sequence differences between α- and γ-synuclein: Implications for fibrillation, *Protein Sci.*, 2006, **15**, 2795–2804.

62 D. H. Kim, J. Lee, K. H. Mok, J. H. Lee and K. H. Han, Salient features of monomeric alpha-synuclein revealed by NMR spectroscopy, *Biomolecules*, 2020, **10**, 1–15.

63 L. M. Reid, I. Guzzetti, T. Svensson, A.-C. Carlsson, W. Su, T. Leek, L. von Sydow, W. Czechtizky, M. Miljak, C. Verma, L. De Maria and J. W. Essex, How well does molecular simulation reproduce environment-specific conformations of the intrinsically disordered peptides PLP, TP2 and ONEG?, *Chem. Sci.*, 2022, **13**, 1957–1971.

64 M. Bisaglia, I. Tessari, S. Mammi and L. Bubacco, Interaction between α-synuclein and metal ions, still looking for a role in the pathogenesis of Parkinson's disease, *NeuroMolecular Med.*, 2009, **11**, 239–251.

65 M. Chwastyk and M. Cieplak, Conformational Biases of α-Synuclein and Formation of Transient Knots, *J. Phys. Chem. B*, 2020, **124**, 11–19.

66 V. T. Duong, Z. Chen, M. T. Thapa and R. Luo, Computational Studies of Intrinsically Disordered Proteins, *J. Phys. Chem. B*, 2018, **122**, 10455–10469.

67 P. Robustelli, S. Piana and D. E. Shaw, Developing a molecular dynamics force field for both folded and disordered protein states, *Proc. Natl. Acad. Sci. U. S. A.*, 2018, **115**, E4758–E4766.

68 K. Q. Hoffmann, M. McGovern, C. C. Chiu and J. J. De Pablo, Secondary structure of rat and human amylin across force fields, *PLoS One*, 2015, **10**, 1–24.

69 D. A. Case, I. Y. Ben-Shalom, S. R. Brozell, D. S. Cerutti, I. T.E. Cheatham, V. W. D. Cruzeiro, T. A. Darden, R. E. Duke, D. Ghoreishi, G. Giambasu, T. Giese, M. K. Gilson, H. Gohlke, A. W. Goetz, D. Greene, R. Harris, N. Homeyer, Y. Huang, S. Izadi, A. Kovalenko, R. Krasny, T. Kurtzman, T. S. Lee, S. LeGrand, P. Li, C. Lin, J. Liu, T. Luchko, R. Luo, V. Man, D. J. Mermelstein, K. M. Merz, Y. Miao, G. Monard, C. Nguyen, H. Nguyen, A. Onufriev, F. Pan, R. Qi, D. R. Roe, A. Roitberg, C. Sagui, S. Schott-Verdugo, J. Shen, C. L. Simmerling, J. Smith, J. Swails, R. C. Walker, J. Wang, H. Wei, L. Wilson, R. M. Wolf, X. Wu, L. Xiao, Y. Xiong, D. M. York and P. A. Kollman, *AMBER 2019*, San Francisco, 2019.

70 R. Zhou and B. J. Berne, Can a continuum solvent model reproduce the free energy landscape of a -hairpin folding in water?, *Proc. Natl. Acad. Sci.*, 2002, **99**, 12777–12782.

71 U. R. Shrestha, J. C. Smith and L. Petridis, Full structural ensembles of intrinsically disordered proteins from unbiased molecular dynamics simulations, *Commun. Biol.*, 2021, **4**, 1–8.

72 S. Bhattacharya, L. Xu and D. Thompson, Long-range Regulation of Partially Folded Amyloidogenic Peptides, *Sci. Rep.*, 2020, **10**, 1–17.

73 H. T. Li, H. N. Du, L. Tang, J. Hu and H. Y. Hu, Structural transformation and aggregation of human α-synuclein in trifluoroethanol: Non-amyloid component sequence is essential and β-sheet formation is prerequisite to aggregation, *Biopolymers*, 2002, **64**, 221–226.